Inorganic Chemistry
Article
Cite This: Inorg. Chem. XXXX, XXX, XXX−XXX
pubs.acs.org/IC

Investigation of Factors That Affect the Oxidation State of Ce in the Garnet-Type Structure

Rahin Sifat, Jeremiah C. Beam, and Andrew P. Grosvenor*

Department of Chemistry, University of Saskatchewan, Saskatoon, Saskatchewan, S7N 5C9 Canada

S *Supporting Information*

ABSTRACT: Oxide materials that adopt the garnet-type structure ($X_3A_2B_3O_{12}$) have received attention for a wide variety of applications, one of which is as potential wasteforms for the sequestration of radioactive actinide elements. The actinides are able to be accommodated in the eight-coordinate X site of the garnet structure. This study focuses on the investigation of Ce substitution into the X site as a surrogate for Pu because of their similar chemical properties. This is accomplished through analysis of the $Y_{3-z}Ce_zAlFe_4O_{12}$ ($0.05 \leqslant z \leqslant 0.20$) materials. The effects of the Ce concentration, oxidation state of the Ce in the starting materials, annealing environment, and cooling rate on the local structure and Ce and Fe oxidation states were investigated through analysis of the powder X-ray diffraction patterns and Ce L_3-edge and Fe K-edge X-ray absorption spectroscopy (XANES) spectra. Analysis of Ce L_3-edge XANES spectra indicated that Ce was present as both 3+ and 4+ oxidation states, the ratios of which depended on the synthetic conditions. The largest concentration of Ce^{4+} was observed when the materials were postannealed at 800 °C following synthesis of the materials at 1400 °C. Variations in the Ce oxidation state are the result of the temperature-dependent Ce^{3+}/Ce^{4+} redox couple, with Ce^{4+} being favored at lower temperatures. Analysis of the Fe K-edge spectra indicated that Fe was only present in the 3+ oxidation state and the Fe coordination number increased with increasing concentration of Ce^{4+}, which is necessary to charge balance the system. The materials in this study can be described as an oxygen-intercalated garnet-type structure with the formula $Y_{3-z}Ce_zAlFe_4O_{12+\delta}$.

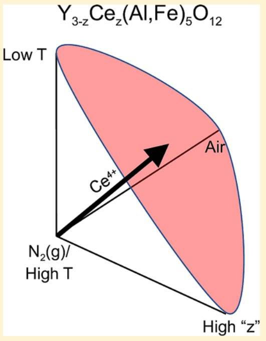

1. INTRODUCTION

Materials that adopt the garnet-type structure have received attention for a range of technological applications (e.g., microwave optical elements, computer memory, solid-state lasers, and magnetic materials) as well as potential host matrixes for nuclear waste.[1−6] This structure has the general formula $X_3A_2B_3O_{12}$ where X, A, and B indicate (Figure 1), respectively, the eight-coordinate dodecahedral, six-coordinate octahedral, and four-coordinate tetrahedral sites in the cubic system.[7] The A site (tetrahedra) and B site (octahedra) share corners and form chains in the ⟨100⟩ direction. They also form a three-dimensional framework by sharing edges with the X site.[8,9] Materials adopting the garnet-type structure have the space group *Ia-3d* with 8 formula units per unit cell. It has been found that, among these three polyhedra, the eight-coordinate X site and six-coordinate A site can be occupied by large cations with oxidation states varying from 2+ to 4+. (e.g., Ca, Ce, Th, and U).[5,6,10−12]

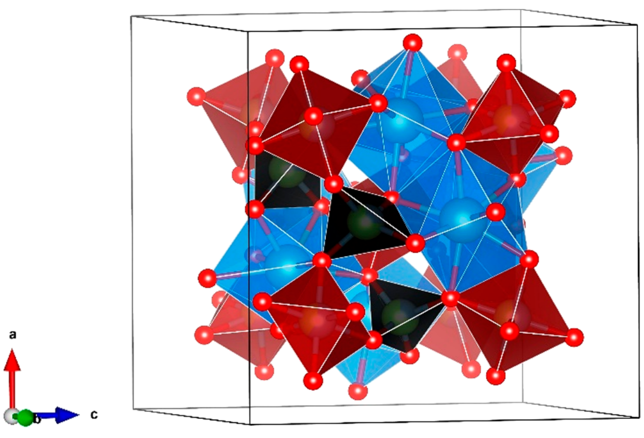

Figure 1. Schematic representation of the garnet crystal structure. Blue, red, and black polyhedra represent the eight-, six-, and four-coordinate sites, respectively.

Studies of natural uranium-bearing garnet minerals such as Zr-containing elbrusite ($Ca_3UZrFe_3O_{12}$; ∼27 wt % U) suggest that the garnet-type structure has good long-term stability.[13] The high loading of U within this phase also suggests the potential of materials adopting the garnet-type structure to be nuclear waste forms. It is notable that garnet-type materials have been synthesized that contain a high concentration of U (∼30 wt % U).[12,14,15] A considerable amount of work has been completed to study the stability of actinides in garnet against radiation damage and corrosion resistance.[6,16−18] However, factors that affect the oxidation states in garnet-type oxides have not been addressed. The incorporation of radioactive actinides with varying oxidation states into nuclear wasteforms is also of importance.[10,17,19−21] The substitution of U or Pu into garnet is complex because of the variable oxidation states of these

Received: September 3, 2018

elements, which can be studied by investigating Ce-containing garnet-type materials because Ce behaves in a manner similar to that of some actinide elements (e.g., Pu).[22,23]

Ce-substituted garnet-type materials, $Y_{3-z}Ce_zAlFe_4O_{12}$, were investigated in this study. The objective of this investigation was to understand the effect of substituting Ce with different oxidation states into the X site in the garnet-type structure. Four different sets of garnet-type ($Y_{3-z}Ce_zAlFe_4O_{12}$; $0.05 \leq z \leq 0.20$) materials were synthesized, followed by analysis of the powder X-ray diffraction (XRD) patterns and Ce L_3-edge and Fe K-edge X-ray absorption near-edge spectroscopy (XANES) spectra to study the effects of the starting materials, annealing temperatures, cooling rates, and annealing environments on the crystal structure and electronic structures of these materials. Ce L_3-edge and Fe K-edge XANES spectra were collected to study how the Ce and Fe oxidation states changed in this system and to investigate if changes in the local structure occur.

2. EXPERIMENTAL SECTION

2.1. Synthesis and Powder XRD. The $Y_{3-z}Ce_zAlFe_4O_{12}$ ($0.05 \leq z \leq 0.20$) materials were prepared using the traditional ceramic method. Four sets of samples were synthesized using differing starting materials, annealing environments, and cooling rates after high-temperature annealing. Details of the synthesis of the four different sets of garnet materials are presented in Table 1. Stoichiometric amounts of CeO_2 (Alfa Aesar; 99.9%), Al_2O_3 (Alfa Aesar; 98%), Fe_2O_3 (Alfa Aesar; 99.945%), and Y_2O_3 (Alfa Aesar; 99.99%) were mixed and then heated under air at 1400 °C to produce samples for set 1. The materials were held at 1400 °C for 9 days with intermittent quenching, grinding, and repelleting. Once the reaction was complete, the samples from set 1 were quenched in air. As indicated in Table 1, stoichiometric amounts of $Ce(NO_3)_3{\cdot}6H_2O$ (Alfa Aesar; 99.5%), Al_2O_3 (Alfa Aesar; 98%), Fe_2O_3 (Alfa Aesar; 99.945%), and Y_2O_3 (Alfa Aesar; 99.99%) were used as starting materials for sets 2–4. The annealing environments and cooling rates after annealing were the same for sets 1 and 2. Samples from set 3 were annealed under air at 1400 °C and then slow-cooled to room temperature, while samples from set 4 were annealed at 1400 °C under $N_2(g)$ (Praxair; 99.995%) and then slow-cooled to room temperature under the same conditions. The starting materials were mechanically mixed in the appropriate stoichiometries using a mortar and pestle and pressed into pellets at 6 MPa. The pellets were heated at 1400 °C under different conditions (depending on the set) for 9 days and then cooled to room temperature using different cooling rates. Intermediate grinding and pelleting of the materials were performed every 3 days to improve the homogeneity of the materials. Two samples from each set were postannealed (PA) at 800 °C for 48 h followed by the cooling rate assigned for each set. Phase analysis of the materials was performed using powder XRD. The powder XRD patterns were collected using a PANalytical Empyrean or Rigaku Ultima IV powder diffractometer equipped with a Cu Kα X-ray source. Rietveld refinement was performed using the X'Pert *HighScore Plus* software program from PANalytical. The following parameters were refined in the following order: background, scale factor, zero shift, lattice constant (a), Caglioti scattering parameters (U, V, and W), peak shape, and Rietveld asymmetry profile variables.

Table 1. Labels and Descriptions of the Different Samples Studied

assigned set	starting materials	annealing condition at 1400 °C	cooling rate after annealing
set 1	CeO_2, Al_2O_3, Fe_2O_3, and Y_2O_3	annealed under air	quenched in air
set 2	$Ce(NO_3)_3{\cdot}6H_2O$, Al_2O_3, Fe_2O_3, and Y_2O_3	annealed under air	quenched in air
set 3	$Ce(NO_3)_3{\cdot}6H_2O$, Al_2O_3, Fe_2O_3, and Y_2O_3	annealed under air	slow cooled to room temperature
set 4	$Ce(NO_3)_3{\cdot}6H_2O$, Al_2O_3, Fe_2O_3, and Y_2O_3	annealed under $N_2(g)$	slow cooled to room temperature

2.2. XANES. Ce L_3-edge and Fe K-edge XANES spectra were collected at the Advanced Photon Source (APS) using the Sector 20 bending magnet beamline (20-BM; CLS@APS) and a Si (111) crystal monochromator.[24] All spectra were collected using an energy step size of 0.15 eV/step through the absorption edge. Cr metal was used as a reference for the Ce L_3-edge XANES spectra, with the absorption edge energy set to 5989 eV.[25] Fe metal foil was used as a reference, with the absorption edge energy set to 7112 eV for the Fe K-edge XANES spectra.[25] The resolution of the spectra was 0.8 eV at 5723 eV (Ce L_3-edge) and 0.9 eV at 7112 eV (Fe K-edge). Samples were prepared by spreading a thin layer of finely ground powder between the Kapton tape. The thickness was adjusted by adding or removing layers to ensure uniform absorption of X-rays by the materials. Multiple scans were collected in both the fluorescence yield and transmission mode. The transmission spectra were collected using an ionization chamber filled with 100% $N_2(g)$ to achieve optimal absorption-edge heights. Ce L_3-edge XANES spectra were fitted using a linear combination fit (LCF) of two standard materials. $CePO_4$ was used as a standard for Ce^{3+}, and $Gd_2Ce_2O_7$ was used as a standard for Ce^{4+}. The spectra were fitted from 20 eV below the main absorption edge (5725 eV) to 30 eV above the absorption edge. All spectra were calibrated, normalized, and analyzed using the *Athena* software program.[26] This program was also used to perform the linear combination fitting of the Ce L_3-edge XANES spectra.

3. RESULTS AND DISCUSSION

3.1. Powder XRD. Powder XRD patterns were collected from all synthesized samples and are shown in Figure 2. The formation of phase-pure garnet-type oxides was confirmed for the $Y_{3-z}Ce_zAlFe_4O_{12}$ ($0 \leq z \leq 0.20$) materials, and no secondary phases were detected. While the synthetic and annealing conditions in these materials were quite different, there was almost no change in their lattice parameters (Table S1). Postannealing of the materials at 800 °C was conducted to observe the effect of the temperature on the Ce oxidation state. The XRD patterns from these PA phases and the as-synthesized materials showed no comparable differences. All materials presented in this study have powder XRD patterns that are consistent with those expected for materials that adopt the garnet-type structure having a similar composition.[27]

Rietveld refinement of $Y_{2.80}Ce_{0.20}AlFe_4O_{12}$, which was synthesized using a Ce^{3+} starting material, annealed in air, and quench-cooled, was performed to see how well the experimental patterns agreed with the calculated pattern of a Ce-doped garnet structure. The model system, $Y_{2.80}Ce_{0.20}AlFe_4O_{12}$, was based on $Y_3AlFe_4O_{12}$, with Ce substituting for Y in the eight-coordinate X site of the garnet structure.[28] The structural parameters and refinement results are presented in Table S2. The atomic coordinates, site occupancies, and overall isotropic thermal factor (B_{OVL}) were held constant. The results of the refinement are presented in Figure 3, which indicate that the model system compares well with the experimental results.

3.2. Ce L_3-Edge XANES Spectra. Ce L_3-edge XANES spectra were collected from all samples to determine how the Ce oxidation state changed depending on the concentration and synthesis conditions and are presented in Figure 4. The spectra show two distinct features resulting from 2p → 4f/5d excitations.[11,23,29,30] Changes in the line shape, onset energy of the absorption edge, and intensity of spectral features are observed with variations in the Ce oxidation state (4+ vs 3+).[23,29−31] As the oxidation state increases, fewer electrons are available to screen the nuclear charge. This leads to an increase

DOI: 10.1021/acs.inorgchem.8b02506
Inorg. Chem. XXXX, XXX, XXX−XXX

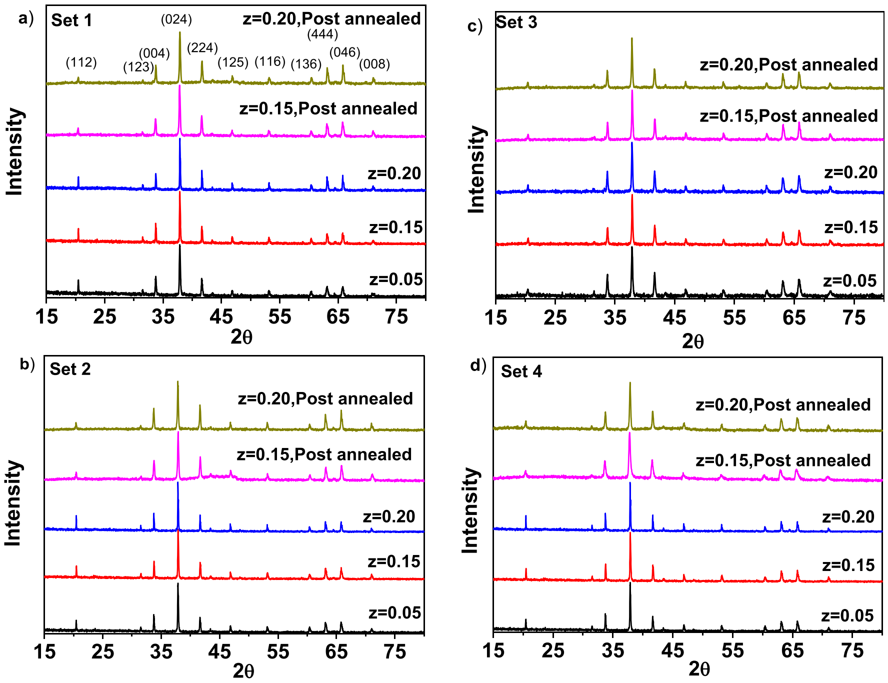

Figure 2. Powder XRD patterns collected from $Y_{3-z}Ce_zAlFe_4O_{12}$: (a) set 1; (b) set 2; (c) set 3; (d) set 4. Set descriptions are given in Table 1.

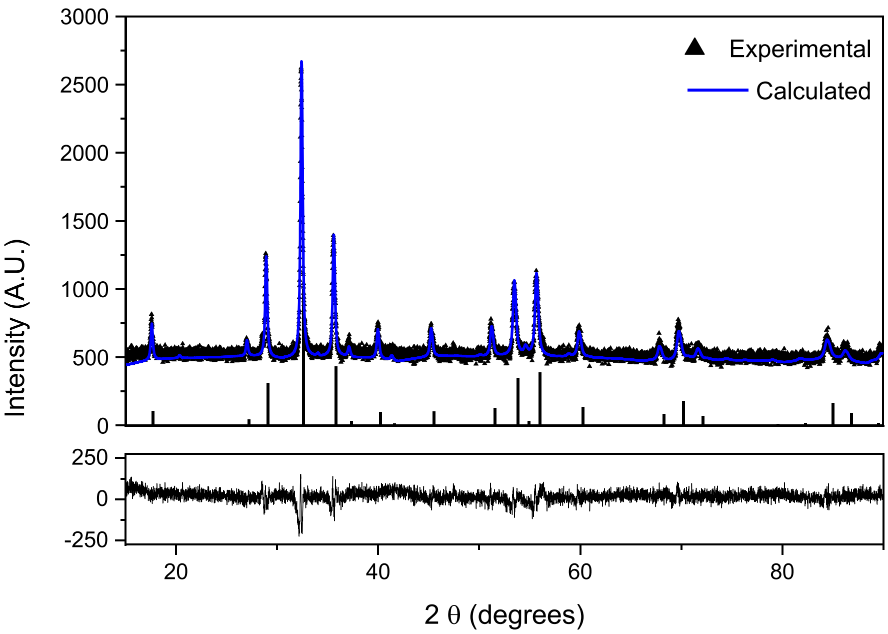

Figure 3. Rietveld refinement of $Y_{2.80}Ce_{0.20}AlFe_4O_{12}$ synthesized using a Ce^{3+} starting material, annealed under N_2(g), and slow-cooled to room temperature. Triangles indicate the experimental data, the blue line indicates the calculated pattern, and the black lines indicate the allowed reflections and expected peak intensity ratios. The difference plot is given below the Rietveld plot.

in the energy required to excite core electrons, which results in an increase in the observed absorption energy of the XANES spectra.[30−33−] Spectra from Ce^{4+}-containing materials contain four features because of one preedge quadrupolar 2p → 4f transition and three dipolar 2p → 5d transitions that result from changes in the Ce 4f final-state occupancies (i.e., $4f^2$, $4f^1$, $4f^0$).[23,30,34,35] The excitation of a 2p electron from Ce^{3+} only results in one intense peak being observed in the Ce L_3-edge XANES spectra.[31] Examination of the spectra in Figure 4 shows two dominant features at different energies, which indicate the presence of trivalent and tetravalent Ce.[11,29,31] The peak at ~5727 eV corresponds primarily to Ce^{3+}, while the peak at ~5737 eV corresponds to Ce^{4+}.

A comparison of the normalized Ce L_3-edge XANES spectra (Figure 4) of the as-synthesized and PA samples showed changes in the line shape. The intense feature located at ~5727 eV indicates the presence of Ce^{3+} as the major oxidation state for all samples. The Ce L_3-edge XANES spectra from sets 1−3 show an increase in the intensity of the Ce^{4+} feature in the spectra from the PA samples. The temperature-dependent Ce^{3+}/Ce^{4+} redox couple ($2Ce^{4+} + O^{2-} \rightleftharpoons 2Ce^{3+} + {}^{1}/_{2}O_2$) is responsible for the change in the oxidation state from Ce^{3+} to Ce^{4+} observed in the

DOI: 10.1021/acs.inorgchem.8b02506
Inorg. Chem. XXXX, XXX, XXX−XXX

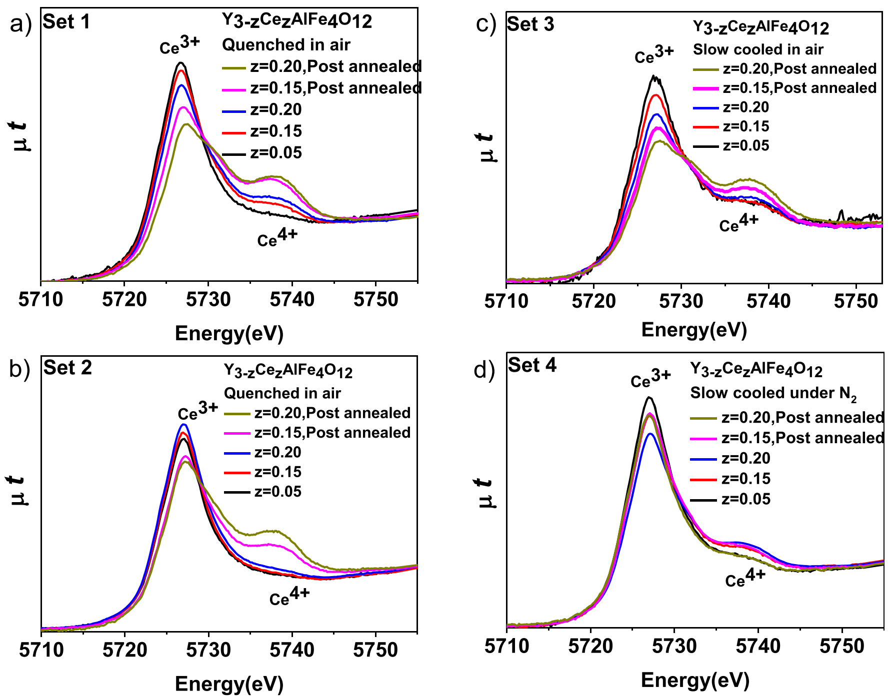

Figure 4. Normalized Ce L_3-edge XANES spectra from $Y_{3-z}Ce_zAlFe_4O_{12}$: (a) set 1 materials were synthesized using a Ce^{4+}-containing starting material and quenched in air; (b) set 2 materials were synthesized using a Ce^{3+}-containing starting material and quenched in air; (c) set 3 materials were synthesized using a Ce^{3+}-containing starting material and slow-cooled in air; (d) set 4 were synthesized using a Ce^{3+}-containing starting material and slow-cooled under N_2.

PA samples.[23,36] As the temperature decreases, the equilibrium shifts toward Ce^{4+}.[23,36] The incorporation of Ce^{4+} into the garnet structure does not result in any structural changes, as observed from the powder XRD patterns of the PA samples, demonstrating the structural integrity of the garnet-type structure. Charge balancing of the garnet structure with Ce^{4+} incorporation can be maintained by reducing Fe^{3+} to Fe^{2+} (which has been suggested previously)[10,29,37] or by incorporating more O into the structure. This is further explored below during the discussion of the Fe K-edge XANES spectra (see section 3.3)

As indicated above, Ce L_3-edge XANES spectra result (primarily) from the excitation of 2p electrons to 5d states and are very sensitive to variations in the oxidation state. It is observed in Figure 4 that, as the degree of Ce substitution in the garnet system increases, so does the average oxidation state of the Ce. The PA samples have a higher average Ce oxidation state, and the Ce^{3+}/Ce^{4+} ratio also depends on the amount of Ce incorporation in the system. Linear combination fitting of the Ce L_3-edge XANES spectra was performed to quantify the relative amounts of Ce^{3+} and Ce^{4+} present in each of the garnet materials, and the results are presented in Table 2. In set 1 (Figure S1), the amount of Ce^{4+} increases as the amount of Ce substituted into the garnet structure increases. Additionally, postannealing of these materials at 800 °C increases the amount of Ce^{4+} present. This trend is also seen in set 2 (Figure S2) and set 3 (Figure S3), with the amount of Ce^{4+} increasing in each sample after postannealing at 800 °C. This is expected as the temperature-dependent redox couple favors Ce^{4+} at lower temperatures. Set 4 (Figure S4), however, does not follow a trend with regard to the amount of Ce^{4+} increasing after postannealing. This can be attributed to the importance of the partial pressure of O on the temperature-dependent Ce^{3+}/Ce^{4+} redox couple. Normalized Ce L_3-edge XANES spectra from

Table 2. LCF Results of the Ce L_3-Edge XANES Spectra[a]

	Ce^{3+} (%)	Ce^{4+} (%)
	Set 1	
z = 0.20, PA	42	58
z = 0.15, PA	55	45
z = 0.20	73	27
z = 0.15	84	16
z = 0.05	99	1
	Set 2	
z = 0.20, PA	51	49
z = 0.15, PA	60	40
z = 0.20	87	13
z = 0.15	94	6
z = 0.05	90	10
	Set 3	
z = 0.20, PA	37	63
z = 0.15, PA	56	44
z = 0.20	58	42
z = 0.15	69	31
z = 0.05	81	19
	Set 4	
z = 0.20, PA	87	13
z = 0.15, PA	74	26
z = 0.20	67	33
z = 0.15	75	25
z = 0.05	84	16

[a]The error associated with all measurements is ±1%.

$Y_{2.85}Ce_{0.15}AlFe_4O_{12}$ are presented in Figures 5−7 to understand the effect of the staring material, annealing conditions, and cooling rate after annealing, respectively.

Figure 5 contains a comparison that shows the changes in the Ce L_3-XANES spectra based on the oxidation state of the Ce in

DOI: 10.1021/acs.inorgchem.8b02506
Inorg. Chem. XXXX, XXX, XXX−XXX

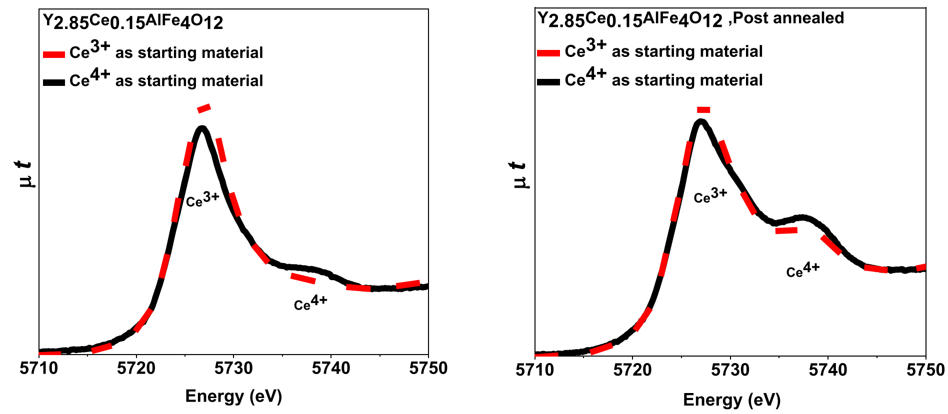

Figure 5. Normalized Ce L_3-edge XANES spectra from $Y_{2.85}Ce_{0.15}AlFe_4O_{12}$ showing the change in the Ce oxidation state that occurs depending on the starting material: (a) as-synthesized samples annealed under the same conditions and then quenched in air directly from 1400 °C; (b) samples that were postannealed at 800 °C.

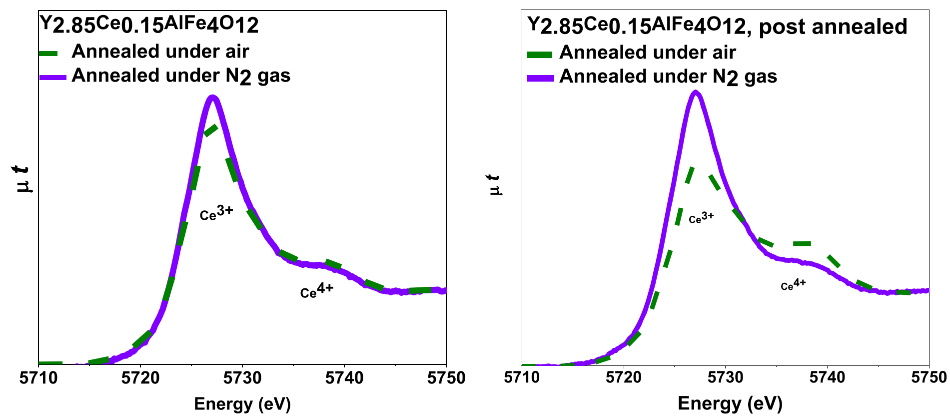

Figure 6. Normalized Ce L_3-edge XANES spectra from $Y_{2.85}Ce_{0.15}AlFe_4O_{12}$ showing the change in the Ce oxidation state that occurs depending on the annealing environment. All materials were synthesized using $Ce(NO_3)_3{\cdot}6H_2O$ as the starting material. (a) Comparison of the spectra from the materials that were synthesized under N_2(g) or air followed by slow cooling to room temperature. (b) Comparison of the spectra from the materials that were synthesized under N_2(g) or air and then postannealed at 800 °C.

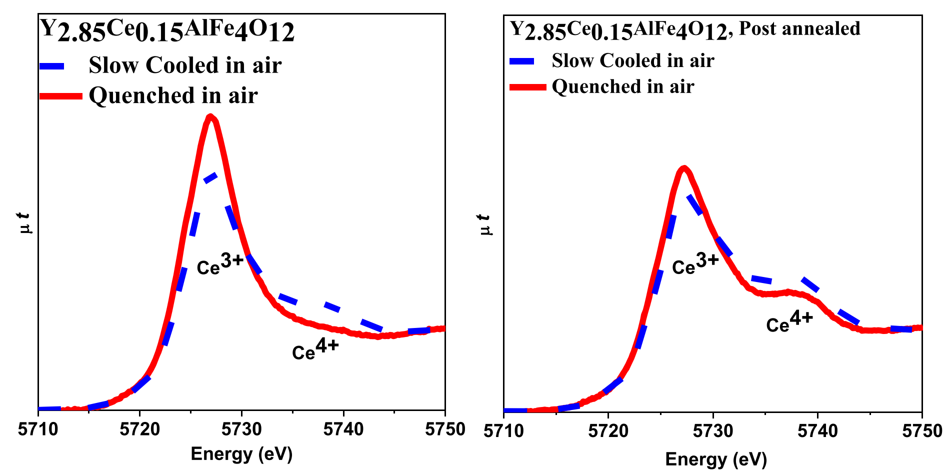

Figure 7. Normalized Ce L_3-edge XANES spectra from $Y_{2.85}Ce_{0.15}AlFe_4O_{12}$ showing the change in the Ce oxidation state that occurs depending on the cooling rate used after high-temperature annealing. All materials were synthesized using $Ce(NO_3)_3{\cdot}6H_2O$ as the starting material. (a) Comparison of the spectra from the materials that were slow-cooled to room temperature versus those that were quenched in air from 1400 °C. (b) Comparison of the spectra from the materials that were postannealed at 800 °C.

the starting material in sets 1 and 2 (see Table 1). As described earlier, the PA samples showed a greater concentration of Ce^{4+} (compared to the as-synthesized materials). Figure 5a compares the spectra from the as-synthesized samples (quenched from 1400 °C to room temperature), while Figure 5b shows the spectra from the samples that were postannealed at 800 °C. These spectra demonstrate that the use of a Ce^{4+}-containing starting material results in a higher average Ce oxidation state.

DOI: 10.1021/acs.inorgchem.8b02506
Inorg. Chem. XXXX, XXX, XXX−XXX

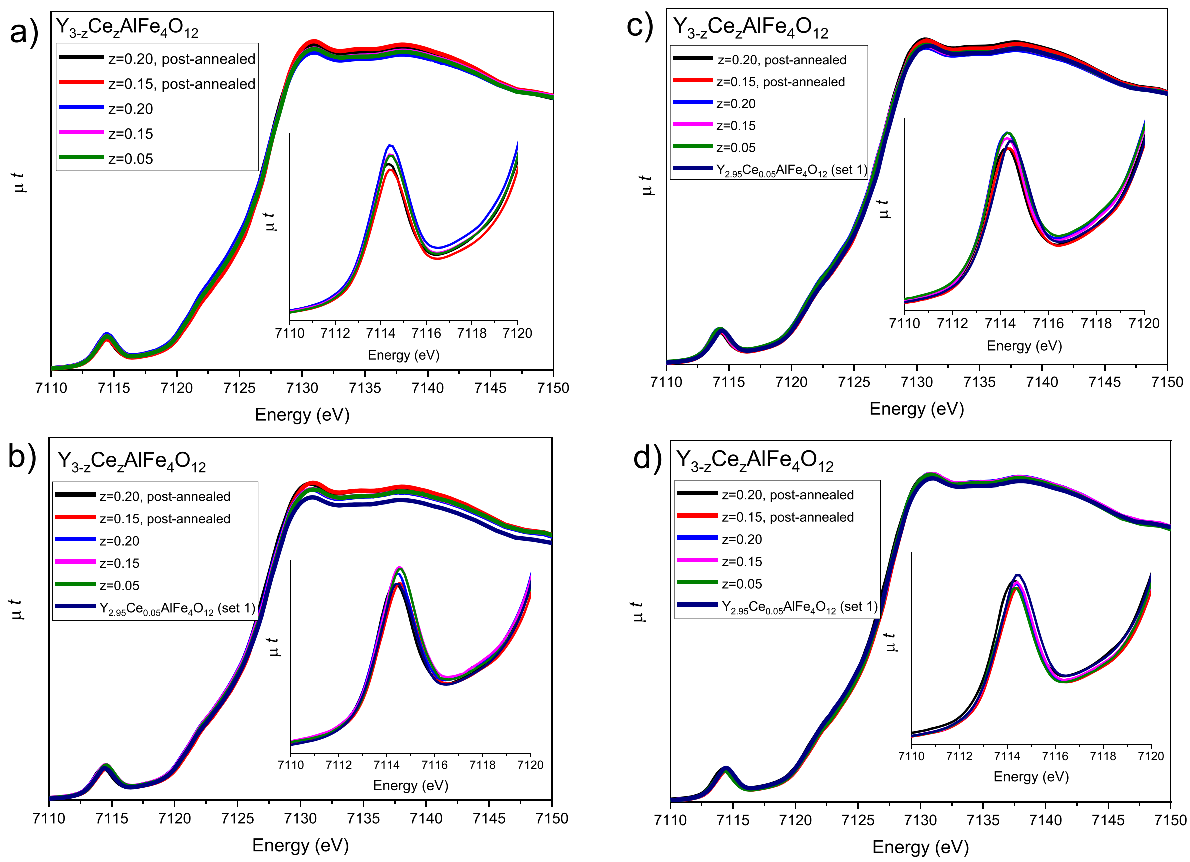

Figure 8. Normalized Fe K-edge XANES spectra. (a) Materials from set 1 were synthesized using a Ce^{4+} starting material and quenched in air. (b) Materials from set 2 were synthesized using a Ce^{3+} starting material and quenched in air. (c) Materials from set 3 were synthesized using a Ce^{3+} starting material and slow-cooled in air. (d) Materials from set 4 were synthesized using a Ce^{3+} material and slow-cooled under $N_2(g)$. The preedge region is highlighted in the inset of each figure. The reference spectrum in sets 2−4 is $Y_{2.95}Ce_{0.05}AlFe_4O_{12}$ from set 1, which was synthesized using a Ce^{4+} starting material and quenched in air. This material was shown to contain no Ce^{4+} by analysis of the Ce L_3-edge XANES spectrum.

The Ce^{3+}/Ce^{4+} ratio in these materials was also observed to vary depending on the oxidation state of the Ce-containing starting material used to synthesize these materials.

The effect of the annealing environment [air vs $N_2(g)$] on the Ce oxidation state is demonstrated by the normalized Ce L_3-edge XANES spectra from $Y_{2.85}Ce_{0.15}AlFe_4O_{12}$ in Figure 6. Annealing under $N_2(g)$ reduces the amount of oxygen present during high-temperature annealing, which creates a reducing environment. The spectral changes observed in Figure 6 indicate that samples annealed under air contain a higher Ce^{4+} concentration than the samples annealed under $N_2(g)$. It can be concluded that the lack of $O_2(g)$ inhibits the temperature-dependent Ce^{3+}/Ce^{4+} redox couple, which results in a lower average Ce oxidation state. However, the spectra presented in Figures 4d and 6 do show that a limited amount of Ce^{4+} was observed in the samples annealed under $N_2(g)$, which is likely a result of the purity of the $N_2(g)$ used and the presence of oxidizing agents in the starting materials such as NO_3^- and H_2O. The observation of a greater concentration of Ce^{4+} in the samples annealed in air versus those annealed in $N_2(g)$ demonstrates the importance of the $O_2(g)$ partial pressure to the average Ce oxidation state in these materials.

Normalized Ce L_3-edge XANES spectra are presented in Figure 7 to understand the effect of the cooling rate on the Ce oxidation state. When the materials that were quench-cooled in air after heating at 1400 °C (as-synthesized) and materials that were slow-cooled to room temperature were compared, the quench-cooled materials contained Ce with a lower average oxidation state. This observation can be explained by the temperature-dependent equilibrium that exists between Ce^{3+} and Ce^{4+}, where the oxidation of Ce^{3+} to Ce^{4+} is an exothermic process.[23,36] As indicated above, the equilibrium shifts toward the more oxidized state when the temperature is lowered. The higher Ce^{4+} concentration observed in the spectra from the slow-cooled samples resulted from exposure of these samples to lower temperatures for longer periods of time.

3.3. Fe K-Edge XANES Spectra. It was demonstrated above by examination of the Ce L_3-edge XANES spectra that the $Y_{3-z}Ce_zAlFe_4O_{12}$ system contains both trivalent and tetravalent Ce and that postannealing of the materials at 800 °C results in an increase in the average Ce oxidation state (compared to the as-synthesized and quench-cooled materials). This observation could imply an increase in the oxygen stoichiometry in the PA materials or that Fe was (partially) reduced from 3+ to 2+ to charge balance the system. The Fe K-edge XANES spectra are sensitive to the oxidation state and coordination number of Fe.[38−40] The normalized Fe K-edge XANES spectra from all four sets of materials investigated are presented in Figure 8. Two unique regions can be observed in the spectra, which are referred to as the preedge region (feature A) and the main-edge region (feature B). The preedge region (feature A) is a result of 1s → 3d transitions, while the main-edge region (feature B) is a result of 1s → 4p transitions.[41,42] A decrease in the intensity of the preedge region indicates an increase of the Fe coordination

DOI: 10.1021/acs.inorgchem.8b02506
Inorg. Chem. XXXX, XXX, XXX−XXX

number, which is accompanied by an increase in the intensity of the main-edge region. Conversely, an increase in the intensity of the preedge region indicates an decrease in the Fe coordination number, which is accompanied by a decrease in the intensity of the main-edge region,[27,40]

The Fe K-edge XANES spectrum collected from $Y_{2.95}Ce_{0.05}AlFe_4O_{12}$, which was synthesized using a Ce^{4+} starting material, annealed under air, and quench-cooled to show a main-edge feature at ~7127 eV and a preedge feature at ~7114 eV, which indicates the presence of Fe^{3+} in the system. This would be expected because the Ce L_3-edge XANES spectrum of this material indicates that Ce exists only as Ce^{3+}, maintaining the charge balancing of this system. The normalized Fe K-edge XANES spectra from $Y_{3-z}Ce_zAlFe_4O_{12}$ (Figure 8) are similar to those found in the spectrum from $Y_{2.95}Ce_{0.05}AlFe_4O_{12}$. This observation confirms that the Fe oxidation state in $Y_{3-z}Ce_zAlFe_4O_{12}$ is 3+ because a (partial) reduction of Fe^{3+} to Fe^{2+} would lead to lower-energy preedge and main-edge features being observed, which was not the case here.[39,41] The normalized Fe K-edge XANES spectra from the set 1−3 PA samples show a decrease in the intensity of the preedge region followed by an increase in the intensity (and slight increase in energy) of the main-edge region, which indicates an increase of the Fe coordination number in the PA samples compared to the as-synthesized materials. This change is subtle in the spectra from the set 2 and 3 samples, while the spectra from set 4 show little to no change. The limited change observed in the Fe K-edge spectra from the set 4 samples is understandable considering that these materials were synthesized under a $N_2(g)$ environment and no significant differences in the Ce L_3-edge spectra from the as-synthesized vs PA samples were observed when the composition was held constant (Figure 4d).

Examination of the Ce L_3-edge XANES spectra presented in Figure 4 established the presence of a higher Ce^{4+} concentration in the PA samples compared to the as-synthesized samples when the materials were annealed in air. The increase in the Fe coordination number observed in the PA samples along with the presence of more Ce^{4+} indicates the presence of excess O in the structure to maintain a charge-balanced system. It is proposed here that the excess O is incorporated into unoccupied interstitial sites in the garnet structure. It should be emphasized that only small changes in the Ce oxidation state were observed along with little to no change in the coordination number of Fe when the system was annealed under $N_2(g)$ (see Figures 4d, 6, and 8). This further indicates the importance of the $O_2(g)$ partial pressure to the oxidation state of Ce observed in these materials and provides more evidence to support the incorporation of excess O in the garnet-type structure to charge balance the (partial) oxidation of Ce^{3+} to Ce^{4+}.

4. CONCLUSIONS

The study has shown by examination of the XANES spectra that $Y_{3-z}Ce_zAlFe_4O_{12}$ contains both Ce^{4+} and Ce^{3+}. Further, it has been shown here that the average oxidation state of Ce in these materials changes depending on the Ce-containing starting material, annealing environment, cooling rate, postannealing treatment, and/or concentration of Ce used to synthesize these materials. Analysis of the Fe K-edge XANES spectra have confirmed the presence of Fe^{3+}. The question then becomes, how do the materials maintain a charge-balanced system? At lower annealing temperatures, the Ce redox couple shifts toward Ce^{4+}, which leads to the incorporation of excess O into the crystal structure to charge balance the system. The increase in the average Fe coordination number in the PA samples, as determined by analysis of the Fe K-edge XANES spectra, confirms the incorporation of excess O in the garnet-type structure. It is proposed here that $Y_{3-z}Ce_zAlFe_4O_{12}$ incorporates excess O into unoccupied interstitial sites to maintain a charge-balanced system, which requires this O-intercalated garnet system to be represented as $Y_{3-z}Ce_zAlFe_4O_{12+\delta}$. The versatility of the garnet structure to be able to incorporate multiple oxidation states of a given element could be important for the sequestration of actinides with easily accessible redox states (e.g., Pu).

■ ASSOCIATED CONTENT

Supporting Information

The Supporting Information is available free of charge on the ACS Publications website at DOI: 10.1021/acs.inorgchem.8b02506.

Lattice constants, Rietveld refinement results, and Ce L_3-edge XANES LCF plots (PDF)

■ AUTHOR INFORMATION

Corresponding Author

*E-mail: andrew.grosvenor@usask.ca.

ORCID

Andrew P. Grosvenor: 0000-0003-0024-0138

Notes

The authors declare no competing financial interest.

■ ACKNOWLEDGMENTS

This project has been funded through a Discovery Grant awarded to APG from the Natural Sciences and Engineering Research Council (NSERC) of Canada. R.S. thanks the University of Saskatchewan for financial support. The Canadian Foundation for Innovation is thanked for funding the purchase of the PANalytical Empyrean powder X-ray diffractometer used in this work. R.S. acknowledges support from the Canadian Light Source (CLS) Graduate and Postdoctoral Student Travel Support Program. Dr. Xiaoxuan Guo, Dr. M. Ruwaid Rafiuddin, Sarah McCaugherty, and Arthur Situm from the Department of Chemistry, University of Saskatchewan, are thanked for help in collecting the XANES spectra presented in this study. Dr. George Sterbinsky, Dr. Tianpin Wu, Dr. Zou Finfrock, and Dr. Mathew Ward are thanked for their support in carrying out XANES experiments at the APS. The CLS is supported by the NSERC, the National Research Council of Canada, the Canadian Institutes of Health Research, the Province of Saskatchewan, the Western Economic Diversification Canada, and the University of Saskatchewan. Sector 20 (CLS@APS) facilities at the APS are supported by the U.S. Department of Energy, Basic Energy Sciences, the CLS and its funding partners, and the APS. Use of the APS, an Office of Science User Facility operated for the U.S. Department of Energy (DOE), Office of Science, by Argonne National Laboratory, was supported by the U.S. DOE under Contract DE-AC02-06CH11357.

■ REFERENCES

(1) Lu, C. H.; Hsu, W. T.; Dhanaraj, J.; Jagannathan, R. Sol−gel pyrolysis and photoluminescent characteristics of europium-ion doped yttrium aluminum garnet nanophosphors. *J. Eur. Ceram. Soc.* **2004**, *24*, 3723−3729.

(2) Batentschuk, M.; Osvet, A.; Schierning, G.; Klier, A.; Schneider, J.; Winnacker, A. Simultaneous excitation of Ce^{3+} and Eu^{3+} ions in $Tb_3Al_5O_{12}$. *Radiat. Meas.* **2004**, *38*, 539−543.
(3) Yen, W. M. General factors governing the efficiency of luminescence devices. *Opt. Mater. (Amsterdam, Neth.)* **2005**, *27*, 1647−1652.
(4) Pari, G.; Mookerjee, A.; Bhattacharya, A. K. First-principles electronic structure calculations of $R_3Al_5O_{12}$ (R being the rare-earth elements Ce−Lu). *Phys. B* **2005**, *365*, 163−172.
(5) Livshits, T. S. Stability of artificial ferrite garnets with actinides and lanthanoids in water solutions. *Geol. Ore Deposits* **2008**, *50*, 470−481.
(6) Yudintsev, S. V.; Osherova, A. A.; Dubinin, A. V.; Zotov, A. V.; Stefanovsky, S. V. Corrosion Study of Actinide Waste Forms with Garnet-Type Structure. *MRS Online Proc. Libr.* **2004**, *824*, XXX DOI: 10.1557/PROC-824-CC8.20.
(7) Menzer, G. Die Kristallstruckture von granat. *Z. Kristallogr.* **1926**, *63*, 157−158.
(8) Novak, A. G.; Gibbs, G. V. The crystal chemistry of the silicate garnets. *Am. Mineral.* **1971**, *56*, 791−823.
(9) Geller, S. Crystal chemistry of the garnets. *Zeitschrift für Krist.* **1967**, *125*, 1−47.
(10) Guo, X.; Rak, Z.; Tavakoli, A. H.; Becker, U.; Ewing, R. C.; Navrotsky, A. Thermodynamics of thorium substitution in yttrium iron garnet: comparison of experimental and theoretical results. *J. Mater. Chem. A* **2014**, *2*, 16945−16954.
(11) Guo, X.; Kukkadapu, R. K.; Lanzirotti, A.; Newville, M.; Engelhard, M. H.; Sutton, S. R.; Navrotsky, A. Charge-Coupled Substituted Garnets ($Y_{3-x}Ca_{0.5x}M_{0.5x}Fe_5O_{12}$) (M = Ce, Th): Structure and Stability as Crystalline Nuclear Waste Forms. *Inorg. Chem.* **2015**, *54*, 4156−4166.
(12) Yudintsev, S. V.; Lapina, M. I.; Ptashkin, A. G.; Ioudintseva, T. S.; Utsunomiya, S.; Wang, L. M.; Ewing, R. C. Accommodation of Uranium into the Garnet Structure. *MRS Online Proc. Libr.* **2002**, *713*, XXX DOI: 10.1557/PROC-713-JJ11.28.
(13) Galuskina, I. O.; Galuskin, E. V.; Armbruster, T.; Lazic, B.; Kusz, J.; Dzierzanowski, P.; Gazeev, V. M.; Pertsev, N. N.; Prusik, K.; Zadov, A. E.; Winiarski, A.; Wrzalik, R.; Gurbanov, A. G. Elbrusite-(Zr)-A new uranian garnet from the Upper Chegem caldera, Kabardino-Balkaria, Northern Caucasus, Russia. *Am. Mineral.* **2010**, *95*, 1172−1181.
(14) Burakov, B. E.; Anderson, E. E.; Zamoryanskaya, M. V.; Petrova, M. A. Synthesis and Study of 239Pu-Doped Gadolinium-Aluminum Garnet. *MRS Online Proc. Libr.* **1999**, *608*, 419.
(15) Zamoryanskaya, M. V.; Burakov, B. E. Cathodoluminescence of Ce, U and Pu in a Garnet Host Phase. *MRS Online Proc. Libr.* **1999**, *608*, 437.
(16) Yudintsev, S. V.; Lizin, A. A.; Livshits, T. S.; Stefanovsky, S. V.; Tomilin, S. V.; Ewing, R. C. Ion-beam irradiation and 244Cm-doping investigations of the radiation response of actinide-bearing crystalline waste forms. *J. Mater. Res.* **2015**, *30*, 1516.
(17) Rak, Z.; Ewing, R. C.; Becker, U. First-principles investigation of Ca3(Ti, Zr, Hf, Sn) 2Fe2SiO12 garnet structure for incorporation of actinides. *Phys. Rev. B: Condens. Matter Mater. Phys.* **2011**, *83*, 1−8.
(18) Utsunomiya, S.; Yudintsev, S.; Ewing, R. C. Radiation effects in ferrate garnet. *J. Nucl. Mater.* **2005**, *336*, 251−260.
(19) Laverov, N. P.; Yudintsev, S. V.; Livshits, T. S.; Stefanovsky, S. V.; Lukinykh, A. N.; Ewing, R. C. Synthetic minerals with the pyrochlore and garnet structures for immobilization of actinide-containing wastes. *Geochem. Int.* **2010**, *48*, 1−14.
(20) Rák, Z.; Ewing, R. C.; Becker, U. Electronic structure and thermodynamic stability of uranium-doped yttrium iron garnet. *J. Phys.: Condens. Matter* **2013**, *25*, 495502.
(21) Rák, Z.; Ewing, R. C.; Becker, U. Role of iron in the incorporation of uranium in ferric garnet matrices. *Phys. Rev. B: Condens. Matter Mater. Phys.* **2011**, *84*, 1−10.
(22) Ewing, R. C.; Weber, W. J.; Lian, J. Nuclear waste disposal-pyrochlore (A 2B 2O 7): Nuclear waste form for the immobilization of plutonium and 'minor' actinides. *J. Appl. Phys.* **2004**, *95*, 5949−5971.
(23) Aluri, E. R.; Bachiu, L. M.; Grosvenor, A. P.; Forbes, S. H.; Greedan, J. E. Assessing the oxidation states and structural stability of the Ce analogue of brannerite. *Surf. Interface Anal.* **2017**, *49*, 1335−1344.
(24) Heald, S. M.; Brewe, D. L.; Stern, E. A.; Kim, K. H.; Brown, F. C.; Jiang, D. T.; Crozier, E. D.; Gordon, R. A. XAFS and micro-XAFS at the PNC-CAT beamlines. *J. Synchrotron Radiat.* **1999**, *6*, 347−349.
(25) Thompson, A.; Attwood, D.; Gullikson, E.; Howells, M.; Kim, K.-J., Kirz, J.; Kortright, J.; Lindau, I.; Peanetta, P.; Robinson, A.; Scofield, J.; Underwood, J.; Vaughan, D.; Williams, G.; Winick, H. *X-ray Data Booklet*; Lawrence Berkeley National Laboratory, University of California: Berkeley, CA, 2001.
(26) Ravel, B.; Newville, M. ATHENA and ARTEMIS Interactive Graphical Data Analysis using IFEFFIT. *Phys. Scr.* **2005**, 1007.
(27) Sifat, R.; Grosvenor, A. P. Examination of the site preference in garnet-type ($X_3A_2B_3O_{12}$X = Y, A/B = Al, Ga, Fe) materials. *Solid State Chemistry* **2018**, *83*, 56−64.
(28) Rodic, D.; Mitric, M.; Tellgren, R.; Rundlof, H. The Cation Distribution and Magnetic Structure of Y3Fe(5-x)AlxO12. *J. Magn. Magn. Mater.* **2001**, *232* (1−2), 1−8.
(29) Guo, X.; Tavakoli, A. H.; Sutton, S.; Kukkadapu, R. K.; Qi, L.; Lanzirotti, A.; Newville, M.; Asta, M.; Navrotsky, A. Cerium substitution in yttrium iron garnet: Valence state, structure, and energetics. *Chem. Mater.* **2014**, *26*, 1133−1143.
(30) Paknahad, E.; Grosvenor, A. P. Investigation of CeTi2O6- and CaZrTi2O7-containing glass- ceramic composite materials. *Can. J. Chem.* **2017**, *95*, 1110−1121.
(31) Huynh, L. T.; Eger, S. B.; Walker, J. D. S.; Hayes, J. R.; Gaultois, M. W.; Grosvenor, A. P. How temperature influences the stoichiometry of CeTi2O6. *Solid State Sci.* **2012**, *14*, 761−767.
(32) Aluri, E. R.; Grosvenor, A. P. A study of the electronic structure and structural stability of Gd2Ti2O7 based glass-ceramic composites. *RSC Adv.* **2015**, *5*, 80939−80949.
(33) Aluri, E. R.; Grosvenor, A. P. An X-ray absorption spectroscopic study of the effect of bond covalency on the electronic structure of Gd2Ti2−xSnxO7. *Phys. Chem. Chem. Phys.* **2013**, *15*, 10477.
(34) Kotani, A.; Kvashnina, K. O.; Butorin, S. M.; Glatzel, P. A new method of directly determining the core−hole effect in the Ce L3 XAS of mixed valence Ce compounds—An application of resonant X-ray emission spectroscopy. *J. Electron Spectrosc. Relat. Phenom.* **2011**, *184*, 210−215.
(35) Nachimuthu, P.; Shih, W.-C.; Liu, R.-S.; Jang, L.-Y.; Chen, J.-M. The Study of Nanocrystalline Cerium Oxide by X-Ray Absorption Spectroscopy. *J. Solid State Chem.* **2000**, *149*, 408−413.
(36) Lopez, C.; Deschanels, X.; Bart, J. M.; Boubals, J. M.; Den Auwer, C.; Simoni, E. Solubility of actinide surrogates in nuclear glasses. *J. Nucl. Mater.* **2003**, *312*, 76−80.
(37) Liang, X.; Xie, J.; Deng, L.; Bi, L. First principles calculation on the magnetic, optical properties and oxygen vacancy effect of $Ce_3Y_{3-x}Fe_5O_{12}$. *Appl. Phys. Lett.* **2015**, *106*, 052401.
(38) Wilke, M.; Farges, F.; Petit, P. E.; Brown, G. E.; Martin, F. Oxidation state and coordination of Fe in minerals: An FeK- XANES spectroscopic study. *Am. Mineral.* **2001**, *86*, 714−730.
(39) Sigrist, J. A.; Gaultois, M. W.; Grosvenor, A. P. Investigation of the Fe K-edge XANES Spectra from $Fe_{1-x}Ga_xSbO_4$: Local versus Nonlocal Excitations. *J. Phys. Chem. A* **2011**, *115*, 1908−1912.
(40) Walker, J. D. S.; Grosvenor, A. P. An X-ray absorption spectroscopic study of the metal site preference in $Al_{1-x}Ga_xFeO_3$. *J. Solid State Chem.* **2013**, *197*, 147−153.
(41) Westre, T. E.; Kennepohl, P.; DeWitt, J. G.; Hedman, B.; Hodgson, K. O.; Solomon, E. I. A multiplet analysis of Fe K-edge 1s → 3d pre-Edge features of iron complexes. *J. Am. Chem. Soc.* **1997**, *119*, 6297−6314.
(42) Wilke, M.; Farges, F.; Petit, P. E.; Brown, G. E.; Martin, F. Oxidation state and coordination of Fe in minerals: An Fe K-XANES spectroscopic study. *Am. Mineral.* **2001**, *86*, 714−730.

DOI: 10.1021/acs.inorgchem.8b02506
Inorg. Chem. XXXX, XXX, XXX−XXX